

## Article

# Study of Reinforced Concrete with the Addition of Pozzolanic against the Penetration of Chlorides through Electrochemical Impedance Spectroscopy

Anilé Ossorio Domínguez <sup>1</sup>, Romildo Dias Toledo Filho <sup>1</sup> , José Antônio da Cunha Ponciano Gomes <sup>2</sup>, Ralph dos Santos Silva <sup>3</sup>, Eduardo Alencar de Souza <sup>2</sup> and Adriana Barbosa da Silva <sup>2,\*</sup>

- <sup>1</sup> Lab NUMATS, Department of Civil Engineering, Federal University of Rio de Janeiro, Rio de Janeiro 21941-598, Brazil; anioosoriobrasil@gmail.com (A.O.D.); toledo@coc.ufrj.br (R.D.T.F.)  
<sup>2</sup> Labcorr, Department of Metallurgical and Materials Engineering, Federal University of Rio de Janeiro, Rio de Janeiro 21941-598, Brazil; ponciano@metalmat.ufrj.br (J.A.d.C.P.G.); eas@metalmat.ufrj.br (E.A.d.S.)  
<sup>3</sup> Lab DME, Department of Mathematic, Federal University of Rio de Janeiro, Rio de Janeiro 21941-598, Brazil; ralph@im.ufrj.br  
\* Correspondence: adrianaiq@gmail.com

**Abstract:** The present work analyzes the behavior in terms of corrosion resistance of three reinforced concrete formulations over a period of 1 year. The samples were subject to a monitoring methodology using the Electrochemical Impedance Spectroscopy (EIE) technique, working only with the real component over time. Three mixtures were used, one conventional without pozzolanic addition (REF) and two others with pozzolanic additions, rice husk ash (RHA) and metakaolin (MK). Prototypes were created and exposed to the action of a 165 g/L NaCl sodium chloride solution. The characterization of the materials was carried out by determining the chloride diffusion profile (ASTM 1556), analyzing images using tomography and with the support of analytical techniques such as X-ray fluorescence and X-ray diffraction. The monitoring methodology using EIE demonstrated the positive effect of the insertion of pozzolans, rice husk ash (RHA) and metakaolin (MK) in delaying the process of chloride diffusion in the concrete, resulting in greater resistance to corrosion. The EIE also showed that the active mineral addition in concrete, resulting in aluminum-silicic composition (MK), had a predominant protective effect on the steel/concrete interface against the attack of chloride ions.

**Keywords:** reinforced concrete; corrosion; chlorides; pozzolan



**Citation:** Domínguez, A.O.; Filho, R.D.T.; Gomes, J.A.d.C.P.; Silva, R.d.S.; de Souza, E.A.; Silva, A.B.d. Study of Reinforced Concrete with the Addition of Pozzolanic against the Penetration of Chlorides through Electrochemical Impedance Spectroscopy. *Constr. Mater.* **2024**, *4*, 194–215. <https://doi.org/10.3390/constrmater4010011>

Received: 20 October 2023  
Revised: 30 November 2023  
Accepted: 14 December 2023  
Published: 2 February 2024



**Copyright:** © 2024 by the authors. Licensee MDPI, Basel, Switzerland. This article is an open access article distributed under the terms and conditions of the Creative Commons Attribution (CC BY) license (<https://creativecommons.org/licenses/by/4.0/>).

## 1. Introduction

Concrete is one of the most widely used materials in the construction industry. The incorporation of reinforcing steel transforms it into a composite material, which has been of significant importance since its initial use in ancient Rome through to the present day. For its proper application, current standards demand adequate performance based on structural parameters, including structural safety, functionality, and durability. These parameters, however, can be compromised over time due to corrosion of the reinforcement.

In addressing the aspect of durability, numerous researchers have demonstrated that the existing criteria for parameterization are not yet sufficient to ensure the service life of concrete structures [1–3]. These criteria are often based merely on minimum cement content, water-to-cement ( $w/c$ ) ratio, porosity, minimal coatings, and certain standards applied to the chloride diffusion process. Such criteria remain inadequate, leading to significant inaccuracies in projecting the service life of structures and supporting alternatives for monitoring and controlling deterioration processes that may affect the material. Thus, they are insufficient for defining the true durability of a structure [4].

As Tutti stated in 1982 [5], the service life of concrete structures can be defined as the period until the breakdown of the passive layer that protects the steel reinforcement

from corrosion. This breakdown is typically caused by the absorption of chlorides, which permeate the concrete from the external environment and reach the reinforcing steel. Similarly, carbon dioxide can reduce the pH of the concrete, thereby compromising the passivation conditions. In light of this, understanding the process of chloride diffusion is crucial for estimating the durability of concrete structures.

Monitoring this process can be effectively achieved using electrochemical techniques, including Electrochemical Impedance Spectroscopy (EIS). Durability criteria can be developed based on parameters obtained through EIS. These parameters provide insights into the progression of the concrete/steel system over time, especially in the presence of chloride ions. Such monitoring allows for the detection of corrosion onset, potentially reducing the uncertainties inherent in predictive durability criteria and supporting correlation with structural integrity analyses.

In addition to Electrochemical Impedance Spectroscopy, other electrochemical techniques are employed to monitor the durability parameters of concrete structures. One such method involves qualitative measurements of the electrochemical potential (E) of steel at its interface with concrete. These measurements can indicate the presence of corrosion and passivation conditions, based on equilibrium thermodynamics principles. Monitoring the evolution of this potential over time, according to the criteria of the ASTM C876 standard, can translate into assessments of corrosion risk.

Another widely used technique is the measurement of polarization resistance, which quantifies the intensity of the corrosion process. This method provides a parameter known as the corrosion current ( $I_{\text{corr}}$ ), leading to an estimation of corrosion rates in mm/year, calculated based on Faraday's law [4].

Corrosion remains a significant threat to structures in coastal areas, primarily due to the presence of chloride ions. This type of corrosion tends to occur rapidly and locally. Once initiated, it is often only detectable by conventional methods at advanced stages, by which time the structure may already be at risk [2]. In this scenario, Electrochemical Impedance Spectroscopy (EIS) becomes increasingly important. EIS is a technique that detects changes in the electrolyte (in this case, the concrete) and in the passive layer formed between the steel and the concrete. It stands out as one of the electrochemical techniques with the highest potential for application and could eventually be employed to monitor the evolution of materials in the field [6].

Considering that EIS is a widely used technique in the field of corrosion and is non-destructive in nature (NDT), it can also be applied in civil construction, particularly regarding corrosion in concrete. EIS provides a set of parameters that, when understood and correlated, have the potential to determine the dynamics of deterioration in concrete structures predictively. This allows for early intervention in structures, before the onset of critical corrosion processes. Additionally, it enables the identification of differences in material behavior, highlighting materials with superior corrosion resistance performance.

As parameters obtained from testing materials under controlled laboratory conditions become more consolidated, they will increasingly support the development of field methods for diagnosing and monitoring structures on a real scale. More consistent results and predictive methods are now available for service life estimation models [6]. The aim of this work is to develop a methodology for monitoring the process of chloride absorption in concrete using Electrochemical Impedance Spectroscopy. This methodology will be used to investigate the process over time, triggered by the absorption of chloride ions, allowing for a comparative identification of the characteristics of conventional concrete and two concretes modified by the addition of active mineral particles (pozzolana).

## 2. Experimental Study

The experimental program of this study was centered around designing and constructing a bench test cell, specifically tailored for Electrochemical Impedance Spectroscopy (EIS) measurements. The setup involved integrating necessary electrochemical instrumentation with a specimen that emulates the geometry of a small-scale reinforced concrete beam. This

specimen was equipped with longitudinal carbon steel bars, compatible for connection to a digital potentiostat. Bars made of CA-50 carbon steel, identical to the reinforcement, served as the working electrode (WE), reference electrode (RE), and counter electrode (CE).

Atop the rectangular bar, a container, or cell, filled with a NaCl solution (concentration of 165 g/L) was installed. This setup, as depicted in Figure 1, facilitates electrochemical measurements over time, employing steel bars as electrodes and concrete as the electrolyte. Chloride ions diffuse through the concrete from the top surface downwards towards the bars acting as working electrodes. This arrangement allows for the evaluation of the electrochemical conditions at the concrete/steel interface and the monitoring of the electrolyte’s evolving characteristics.

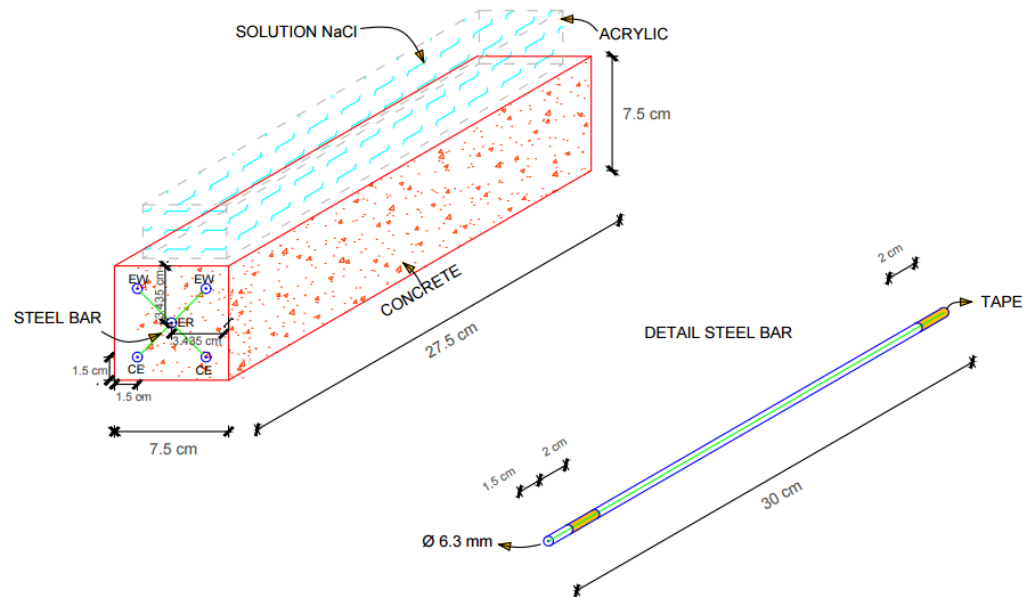


**Figure 1.** Details of the test body used for impedance testing.

Over a period of one year, the evolution of samples from three different concrete types was monitored using the EIS technique. The concretes prepared included one reference sample (REF) without any additions, a second sample with 10% of the cement replaced by rice husk ash (RHA), and a third sample with 10% replacement by metakaolin (MK), both being active mineral additions known as pozzolans.

### 3. Materials and Methods

#### 3.1. Mix Design

The concrete was designed using the methodology recommended by IPT/EPUSP [7]. This approach involves using a mathematical equation derived from the dosing diagram and considering the mortar content to determine the unit weight of each component material (cement, sand, stone). For all mixtures used in this work, a water–cement ratio ( $w/c$ ) of 0.7 was maintained. This high  $w/c$  ratio was chosen to achieve a highly porous microstructure, as the diffusion phenomenon is considerably slower in less porous structures.

The chemical composition of the carbon steel (CA-50S) used in this study is presented in Table 1, as determined by optical emission spectrometry.

**Table 1.** Chemical composition of carbon steel (%).

Element	%
C	0.2370
Si	0.1950
Mn	0.7730
P	0.0044
S	0.0474
Cr	0.0809
Mo	0.0083
Ni	0.0499
Al	0.0221
Co	<0.01
Cu	0.0820
Nb	0.0055
Ti	0.0320
V	<0.001
W	<0.010
Pb	<0.002
Sn	0.0027
Mg	<0.002
B	>0.132
Fe	<98.2

3.1.1. Cement

Initial high strength Portland cement (CP-V ARI HOLCIM) was characterized by X-ray fluorescence analysis. Table 2 shows the chemical composition of the cement obtained by this method.

**Table 2.** Chemical composition of Portland cement CP-V ARI HOLCIM, obtained by X-ray fluorescence (XRF).

FRX	CaO	SiO <sub>2</sub>	Al <sub>2</sub> O <sub>3</sub>	Fe <sub>2</sub> O <sub>3</sub>	MgO	SO <sub>3</sub>	Na <sub>2</sub> O	K <sub>2</sub> O	CaO	SrO	P <sub>2</sub> O <sub>5</sub>	TiO <sub>2</sub>	MnO	PPC
%	63.6	17.6	5.1	2.9	0.72	3.9	0.29	0.85	37.39	0.27	0.27	0.22	0.12	3.9
Bogue Composition	Compound			C <sub>3</sub> S		C <sub>2</sub> S		C <sub>3</sub> A		C <sub>4</sub> AF				
	%			60.15		5.08		8.61		8.82				

Source: CETEM Laboratories–University City/UFRJ.

3.1.2. Pozzolans

Pozzolans are active mineral additions that, when incorporated into Portland cement, can generate the same hydration products as cement. In its chemical composition, its amorphous compounds are responsible for controlling the greater or lesser formation of products by the hydration reaction. In the present study, the mineral additions responsible for the hydration reaction will be reactive silica (SiO<sub>2</sub>) and reactive alumina (Al<sub>2</sub>O<sub>3</sub>) [8].

The results of the structural analysis of the RHA and MK pozzolans are presented in Tables 3 and 4. It was carried out using the Fire Loss X-Ray Fluorescence technique (XRF/DRX).

**Table 3.** FRX of RHA and MK pozzolans.

Density (g/cm <sup>3</sup> ) (He Pic NUMATS)	2.47 @ 21C	2.63 @ 21C
Blaine (cm <sup>2</sup> /g) (NUMATS)	12,246	7004
FRX CETEM (AXIOS Panalytical)	%w/w	%w/w
MgO	0.29	0.81
Al <sub>2</sub> O <sub>3</sub>	0.19	43.5
SiO <sub>2</sub>	93.65	48.5
P <sub>2</sub> O <sub>5</sub>	0.32	0
SO <sub>3</sub>	<0.1	0
K <sub>2</sub> O	1.3	1.8
TiO <sub>2</sub>	0	1.3
Fe <sub>2</sub> O <sub>3</sub>	<0.1	1.9
CaO	0.44	<0.1
MnO	0.29	0
BaO	<0.1	0
Perda ao Fogo	3.5	2.2
Total	100.0	100.0

Source: CETEM Laboratories–University City.

**Table 4.** DRX of RHA and MK pozzolans.

XRD CETEM (Bruker D4)	Tubo Cobalto	Tubo Cobalto
	RHA	MKHPMAX-Co
Phase Name	Wt% in Original sample	Wt% in Original sample
Kaolinite	0.000	5.983
Muscovite	0.000	3.032
Quartz	0.000	6.430
Anatase	0.000	1.051
Zircon	0.000	0.000
Microcline	0.000	3.494
Illite	0.000	14.923
Cristobalite low	5.897	0.000
Fluorite	0.000	0.000
Amorphous	94.1	65.1
-	100.0	100.0

After the characterization of all the materials, also using the IPT/EPUSP method (HELENE and TERZIAN, 1992), the reference trait was determined, with the results shown in Table 5.

**Table 5.** Mix designs based on unit weight.

Cement	M	w/c	Mortar Ratio %	Mix Unit	Slump (cm)	Compressive Strength (MPa)
CP-V ARI HOLCIM	5.94	0.70	53	1:2.679:3.262	12	26
	5.94	0.70	53	1:2.679:3.262:10% RHA	8	28
	5.94	0.70	53	1:2.679:3.262:10% MK	7.5	27

The three concrete mixtures were prepared in a vertical axis mixer. A similar process was followed for producing all three types of concrete, with an additional step of adding

the pozzolanic materials. The densification of the concrete in the molds was performed using a vibrating table. One day after molding, the samples were transferred to a humid chamber (temperature at 24 °C and 70% relative humidity) and left to cure for 28 days. Following this curing period, aged specimens were used for compressive strength tests.

It was decided that for each material, 5 cylindrical specimens (diameter 7.5 cm × height 15 cm) would undergo mechanical testing for resistance to axial compression. For the corrosion study (EIS), 6 prismatic samples (7.5 cm × 7.5 cm × 27.5 cm) were prepared. For the accelerated chloride diffusion test and the tomographic examination, 6 samples for each mix were utilized. In total, 69 concrete samples were employed in the experimental work.

The evaluation of the accelerated chloride diffusion process in the three materials was conducted in accordance with ASTM C 1559 [9]. This standard recommends analyzing a concrete sample exposed to a NaCl environment for a period of 35 days, determining the chloride profiles in 5 g concrete samples extracted from various depths. In this study, a Metrohm Titrando 805 potentiometric titrator (METROHM AG, Herisau, Switzerland) was used for chloride detection and dosing, following the instructions of the AFREM TEST 1999. The free chloride profiles were determined [10]. Subsequently, using mathematical methods implemented in the R computational language, a non-linear regression based on Fick's second law was performed to analytically adjust the free chloride profiles. Finally, the values of the apparent diffusion coefficient ( $D_a$ ) and the surface chloride concentration ( $C_s$ ) for the stipulated exposure time were obtained through optimization, using Equation (1).

$$C_{(x,t)} = C_s - (C_s - C_i) \times \operatorname{erf}\left(\frac{x}{\sqrt{4 \times D_a \times t}}\right) \quad (1)$$

### 3.2. Tomography to Determine Porosity

To determine the porosity of samples subjected to the accelerated test as per ASTM 1556 standards, image processing techniques using tomography were employed. The equipment utilized was a GE-Vtomex/m tomograph with a pixel size of 100 μm. This tomography technique was specifically chosen to preserve the concrete's microstructure, which could be compromised by chloride ion attack, in contrast to conventional tests, like the effective porosity test, which require water and were consequently avoided.

A methodology was developed to perform tomography in a manner compatible with ASTM 1556's accelerated test type, effectively addressing the challenges identified both before and after exposure to chloride ions. Scans were conducted on each sample following the same direction as the diffusion of the chloride ions. Tables quantifying pore descriptor parameters were generated, measuring their occurrence in the materials before and after chloride absorption. These data, derived from image processing, provide valuable parameters that can be correlated with the process of chloride diffusion.

### 3.3. Electrochemical Impedance Spectroscopy—EIS

The EIS tests were conducted following the guidelines of the Spanish standard for accelerated testing of natural chlorides (UNE 83992-1 EX [11]), incorporating certain adaptations in this study, such as sample dimensions, NaCl concentration, and geometry. As illustrated in Figure 1, the steel bars were utilized to construct the working electrochemical cell. The two upper bars served as working electrodes (WEs), the central intermediate bar functioned as the reference electrode (RE), and the two lower bars were employed as counter electrodes (CEs). The frequency sweep for measurement was set from 100 kHz to 10 mHz, with 7 points per decade. The amplitude of the potential signal was 15 mV. The equipment used was AUTOLAB PGSTAT 302 with NOVA 10.1 software. Over the course of one year, we conducted 20 measurements to monitor the progression of three materials, using a NaCl solution with a concentration of 165 g/L as the aggressive agent for each.

Nomenclature was defined to detail the system on the surface of the electrode as shown in Figure 2:

C—Fine Aggregate, Coarse Aggregate, and Concrete;

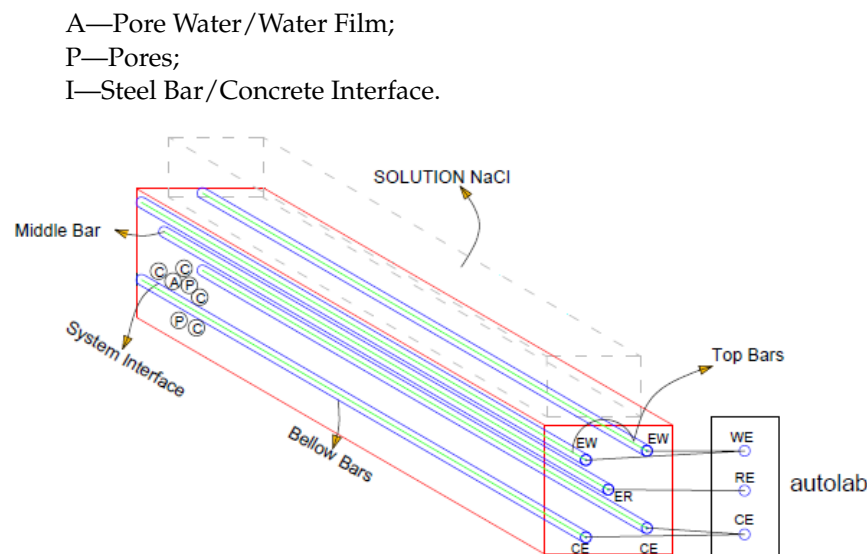


**Figure 2.** Electrochemical cell assembled at AUTOLAB.

Nyquist diagrams, used in Electrochemical Impedance Spectroscopy (METROHM AG, Herisau, Switzerland) for concrete analysis, represent impedance as complex numbers with real ( $Z'$ ) and imaginary ( $Z''$ ) components. In the diagram, the X-axis denotes  $Z'$  (resistive aspects), and the Y-axis represents  $Z''$  (capacitive or inductive behaviors). These plots assist in identifying electrochemical processes in concrete, such as corrosion kinetics and structural integrity. Analyzing frequency responses in Nyquist chloride absorption tests provides insights into the concrete's durability, especially regarding chloride-induced corrosion. This tool is essential in evaluating and developing more durable concrete, resistant to chemical attacks [12].

The use of the Nyquist plot in our study is crucial for understanding the resistance and electrochemical behavior of REF, RHA, and MK concretes, especially in chloride environments. As part of Electrochemical Impedance Spectroscopy (EIS), this technique provides a detailed analysis of the concrete's resistance and reactance, allowing us to quantify how additions like rice husk ash and metakaolin influence corrosion resistance.

The Nyquist plots reveal the kinetics of corrosion at the microstructural level and are essential for understanding the deterioration mechanisms and the effectiveness of mineral additions in enhancing concrete durability. They offer insights into the interactions between concrete and the corrosive environment, highlighting the importance of physicochemical reactions in corrosion resistance.

In summary, the Nyquist method enriches our analysis, providing a deeper understanding of the processes occurring in concrete under corrosive conditions and the efficacy of mineral additions in protecting against corrosion.

## 4. Results and Discussion

### 4.1. Accelerated Test of Chlorides According to ASTM 1556

Table 6 displays the results of chloride absorption tests for the three types of concrete studied (REF, MK, RHA), following the ASTM C 1556 standard procedures. The surface chloride concentration ( $C_s\%$ ) was calculated based on the concrete's weight, using 5 g of solute as outlined in AFREM TEST 1999. From the free chloride profile, shown in Figure 3, the apparent diffusion coefficient ( $D_a$ ) was derived, with its values provided below.

**Table 6.** Chloride absorption tests.

Deep (mm)	Ref-N (mg/L)	RHA(mg/L)	MK (mg/L)
0–5	0.500	0.812	0.804
5–10	0.384	0.388	0.296
10–15	0.268	0.188	0.096
15–20	0.200	0.104	0.080
20–25	0.164	0.080	0.032
25–30	0.140	0.060	0.024
30–35	0.132	0.052	0.020
$D_a$ (m <sup>2</sup> /s)	$8.45 \times 10^{-11}$	$1.63 \times 10^{-11}$	$9.29 \times 10^{-12}$
$C_s$ (%)	0.5653683	1.240761	1.49701

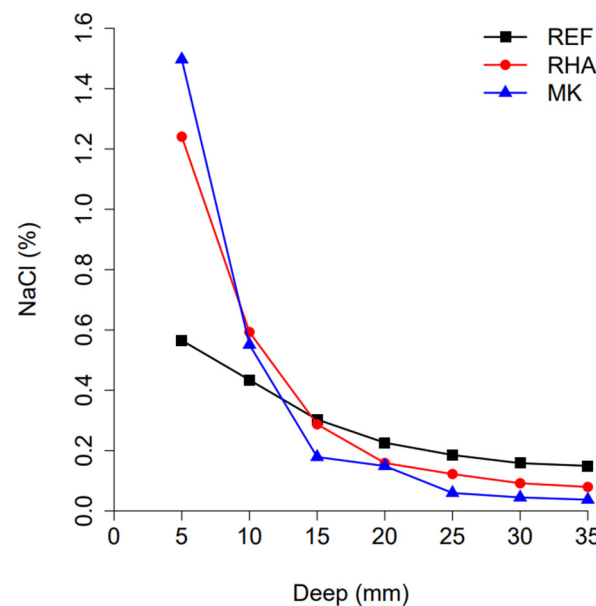


**Figure 3.** The apparent diffusion coefficient,  $D_a$ .

The results show that the highest apparent diffusion coefficient is for Portland cement concrete without REF addition, recorded  $8.45 \times 10^{-11} \text{ m}^2/\text{s}$ . The diffusion coefficient in concrete with rice husk ash (RHA) addition is  $1.63 \times 10^{-11} \text{ m}^2/\text{s}$ , while the lowest value is observed in concrete with metakaolin (MK) addition, at  $9.29 \times 10^{-12} \text{ m}^2/\text{s}$ .

It is important to note that in each material studied, chloride anions exist in different states within the concrete. Some free chlorides are dissolved in the liquid phase of the concrete pores, while others are physically restrained, unable to penetrate the reinforcement. These chlorides may also be physically adsorbed on the pore surface via Van der Waals forces or chemically bound with hydration compounds in Portland cement [11].

For an initial understanding, consider the conventional reinforced concrete (REF) formulated with Portland cement only. In this material, the defense against chloride ion ingress is effective when the cement contains tricalcium aluminate ( $C_3A$ ) and tetracalcium aluminoferrite ( $C_4AF$ ), which can bind chemically to chloride anions to form Friedel’s salt. This compound is known to reduce the mobility of chloride anions [13].

In RHA concrete, containing silicon-based pozzolans, the protective mechanism is different. In addition to physical barriers, physicochemical interactions create a denser and less porous matrix, reducing the mobility of these anions.

For MK concrete with aluminum-silicate pozzolana, the protection against chloride attack is dual. One mechanism is akin to that in Portland cement. Additionally, the reactive alumina ( $Al_2O_3$ ) in the pozzolan chemically reacts with chlorides, forming Friedel’s salt [13,14].

The results from the diffusion tests in this study align with those in [14]. The pozzolanic additions, especially those based on aluminum and aluminum-silicon, due to their chemical

nature, reduce chloride attacks on steel reinforcement. This effect is not as pronounced with silicon-based pozzolans. The findings underscore the benefits of active mineral additions, particularly aluminum-based ones, in structures exposed to chloride environments, like marine areas. In all three materials, the most significant factor in reducing chloride ion mobility was the chemical nature of the concrete constituents, indicating a stronger chemico-physical interaction than a physico-chemical one.

#### 4.2. Tomography

To gain a deeper understanding of the microstructure of the analyzed concrete, a non-destructive imaging technique (NDT) using a tomograph was employed [15]. This method ensures that the internal structural conditions of the materials remain unchanged. Given that the durability test conducted according to ASTM 1556 involves immersing concrete in sodium chloride, the mercury porosimetry technique was deemed unsuitable. This technique is known to overestimate the volume of fine capillary pores and underestimate that of coarse capillary pores in cement-based systems, though it is still valuable for comparing pore refinement within a system [16,17]. Additionally, the ASTM C642-13 standard-based technique, which measures pore volume, was not used in this study, as it requires water and could obscure the physical changes caused by NaCl absorption in the pores.

Initially, a scan of the cylindrical concrete samples was performed to visualize the pore system in 3D, revealing only the largest pores. To observe the entire pore system, including the smallest pores at approximately 100 μm scale, the highest resolution setting was used [11]. The results are presented in Tables 7–9 for reference concrete (REF), concrete with rice husk ash (RHA) addition, and concrete with metakaolin (MK) addition. This approach also allows for comparisons between concrete samples before and after NaCl exposure [18].

**Table 7.** Number of pores by size range or area in REF concrete before and after chloride absorption.

Interval (mm <sup>2</sup> )	REF Before Chloride (NaCl)	REF After Chloride (NaCl)
0.00–0.13	188,289	112,982
0.13–0.26	108,828	147,894
0.26–0.52	85,360	123,750
0.52–1.05	45,006	53,127
1.05–2.09	18,131	19,609
2.09–4.19	5319	5561
4.19–8.38	503	552
TOTAL	2.48%	2.80%

**Table 8.** Number of pores by size range or area in RHA concrete before and after chloride absorption.

Interval (mm <sup>2</sup> )	RHA Before Chloride (NaCl)	RHA After Chloride (NaCl)
0.00–0.13	35,487	105,340
0.13–0.26	34,256	91,903
0.26–0.52	25,485	49,819
0.52–1.05	15,551	21,077
1.05–2.09	8668	9911
2.09–4.19	2849	3233
4.19–8.38	348	462
8.38–16.75	1	11
16.75–33.5		1
TOTAL	1.06%	1.32%

**Table 9.** Number of pores by size range or area in MK concrete before and after chloride absorption.

Interval (mm <sup>2</sup> )	MK Before Chloride (NaCl)	MK After Chloride (NaCl)
0.00–0.13	64,516	112,982
0.13–0.26	91,914	147,894
0.26–0.52	80,558	123,750
0.52–1.05	42,482	53,127
1.05–2.09	17,430	19,609
2.09–4.19	4864	5561
4.19–8.38	979	552
8.38–16.76	4	-
TOTAL	2.43%	2.60%

The tables illustrate the distribution of pore quantities as a function of the measured pore area before and after NaCl absorption, for scans at 100  $\mu\text{m}$  resolution. A higher frequency of pores was observed with a central value in the range of 8.38 mm<sup>2</sup>, and the smallest number at 0.004 mm<sup>2</sup>. In both cases, the quantity of pores in each range and their total representation in the sample were quantified, with numerical data detailed in Table 7. The data indicate that for the REF concrete without NaCl absorption, the total porosity was 2.48%, which increased to 2.80% after chloride absorption, representing an increase of 11%.

A similar analysis was conducted on the RHA concrete samples, with the results presented in Table 8. This table compares the RHA concrete before and after NaCl absorption. The pore size distribution, determined using a scan with a resolution of 100  $\mu\text{m}$ , revealed the largest pore to be 16.75 mm<sup>2</sup> in the RHA concrete without chloride and 33.5 mm<sup>2</sup> in the concrete post-chloride absorption. The smallest detected pore size was consistent at 0.004 mm<sup>2</sup> for both conditions. Notably, the total porosity of the RHA concrete without chloride was 1.06%, which increased to 1.32% after chloride absorption, signifying a 26% increase.

The results for the MK concrete samples are displayed in Table 9, which covers the MK sample before and after chloride exposure. The total distribution of pore sizes, determined using a scan with a resolution of 100  $\mu\text{m}$ , is also illustrated. The largest pore size detected was 16.76 mm<sup>2</sup> in the MK concrete without chloride absorption, decreasing to 8.38 mm<sup>2</sup> post-absorption. The smallest pore size remained consistent at 0.004 mm<sup>2</sup> under both conditions. Notably, the total porosity of MK concrete without chloride absorption was 2.43%, which increased to 2.60% after chloride exposure, representing a 17% increase.

The reduction in porosity of concrete with pozzolanic additions, compared to standard concrete, can be attributed to the specific physical mechanisms and chemical reactions that occur among the various components of the mixture. These reactions significantly influence the content and nature of the amorphous, glassy, or crystalline fractions, including their silicic or calcareous properties, acidic or basic chemical characteristics, and particle size, among other factors. When considering the behavior of common Portland cement concrete (REF), it is important to note that hydration stimulation occurs directly through a purely physical mechanism: once the cement particles are hydrated, the water fraction is exhausted. The addition of a pozzolanic component to this cement introduces a physicochemical effect, adding a second variant to the hydration stimulation of the cement indirectly [8,19,20].

As a result, concrete with mineral additions, such as RHA and MK concrete, forms a denser matrix compared to REF, thereby enhancing the physical protective effect against chloride ion ingress. Specifically, concrete with silicon-based additions, like RHA, has been observed to be the least porous compared to the aluminum-silicate-based MK concrete, resulting in a matrix with lower porosity [21].

### 4.3. Electrochemical Impedance Spectroscopy

This section presents and discusses the results through Nyquist graphs for the three materials (REF, RHA, MK), utilizing the EIS technique as the basis for obtaining these results, in accordance with the application specifications outlined in Section 3.3.

Figure 4 depicts the Nyquist graph for REF concrete, which was monitored over a period of one year while exposed to NaCl. The spectra for both the first four measurements and the last four are displayed, focusing on the lowest frequency at 10 mHz.

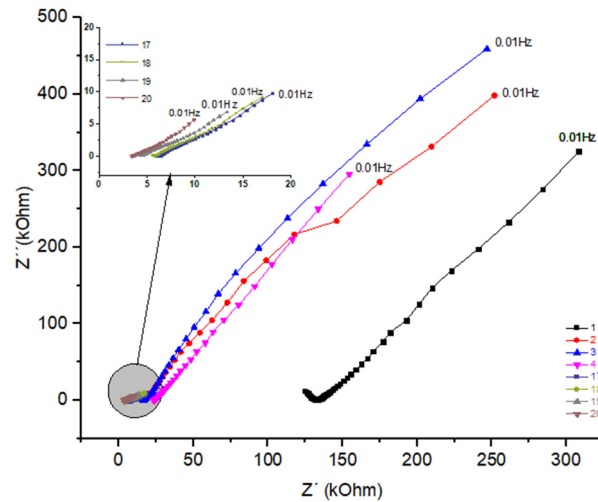


**Figure 4.** Nyquist plot for the REF concrete system over a one-year period of NaCl exposure.

Over time, there is a notable decrease in the real component of impedance, which is attributed to the system’s resistance to the corrosive process induced by NaCl exposure. This decrease is evident when comparing impedances at 10 mHz. For instance, the value of the real component diminishes over time as follows: from 308 kΩ to 154 kΩ, then to 26 kΩ, to 19 kΩ, and finally to 9 kΩ. This significant decrease in system resistance is apparent from the second month of exposure onwards. This trend of a decreasing real component over time is also observed at higher frequencies, as detailed in Table 10. At low frequencies, this is associated with resistance (R4), which reflects the polarization resistance of the electrical charges accumulated by the electrodes, namely the reinforcing bars.

**Table 10.** Real component ( $Z'$ ) for REF concrete associated with system resistance at three frequencies—100 kHz, 39 Hz, and 0.01 Hz.

Frequency/Hz	REF-Months/ $Z'$ kΩ																			
	1	2	3	4	5	6	7	8	9	10	11	12	13	14	15	16	17	18	19	20
100 k	124	15	15	22	14	10	10	10	9	10	10	10	10	8	8	6	5	5	4	3
39	134	17	17	24	15	11	11	11	10	11	11	11	10	9	9	7	6	6	4	3
0.01	308	251	246	154	44	28	27	28	26	26	25	25	24	21	25	19	18	17	13	9

Analyzing the behavior of the material at medium frequencies of the real component, 39 Hz, a similar decrease in system resistance is observed over time, ranging from 134 kΩ to 24 kΩ, then to 11 kΩ, to 7 kΩ, and finally 3 kΩ. This trend may be linked to the resistance of the bar (electrode)/concrete (electrolyte) system, denoted as R2, which appears as a critical point in the spectral analysis.

When examining the imaginary component at 10 mHz, a decrease over time is also observed: from 325 kΩ to 295 kΩ, then to 13 kΩ, to 10 kΩ, and eventually to 5 kΩ. This component, associated with the system’s reactance, indicates opposition to current flow and shows a decrease across all frequencies, as presented in Table 11.

**Table 11.** Imaginary component ( $Z''$ ) for REF concrete associated with system reactance at three frequencies—100 kHz, 39 Hz, and 0.01 Hz.

Frequency/Hz	REF-Months/ $Z''$ k $\Omega$																			
	1	2	3	4	5	6	7	8	9	10	11	12	13	14	15	16	17	18	19	20
100 k	12	0.64	0.68	0.77	0.61	0.45	0.43	0.42	0.33	0.42	0.41	0.33	0.35	0.30	0.22	0.16	0.11	0.09	0.06	0.01
39	1.95	1.10	1.09	0.90	0.64	0.44	0.45	0.41	0.38	0.38	0.38	0.36	0.33	0.32	0.34	0.29	0.28	0.27	0.25	0.19
0.01	325	398	459	295	32	14	12	13	13	13	12	12	12	10	13	10	9.74	9.13	6	5

The behavior described above for the real component, associated with system resistance, is visually represented in Figure 5. This figure illustrates the decreasing trend of the real component ( $Z'$ ) over time across three selected frequency ranges.

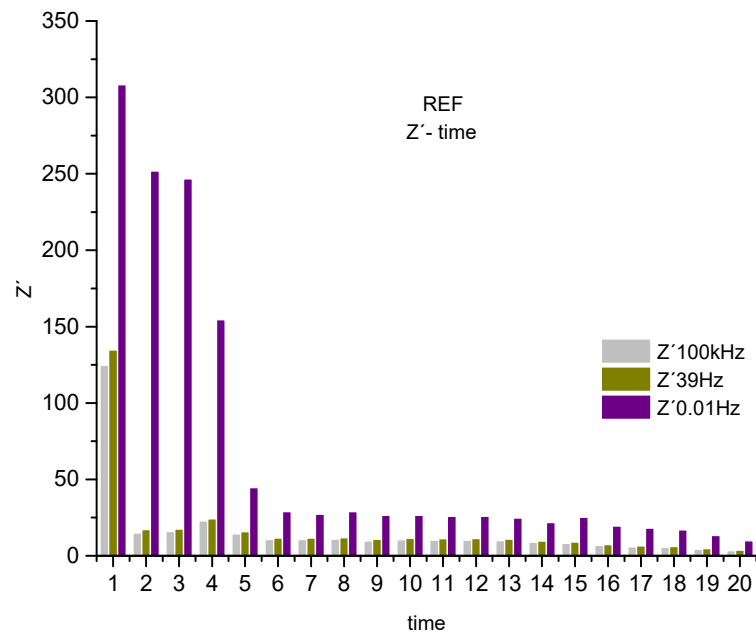


**Figure 5.** Histogram of the real component ( $Z'$ ) for REF concrete, illustrating system resistance at three frequencies—100 kHz, 39 Hz, and 0.01 Hz.

An abrupt drop in the real component, which is associated with the system’s resistance to the corrosive process, is observed at frequencies of 0.01 Hz, 39 Hz, and 100 kHz. This indicates a significant reduction in the system’s resistance to the sweep frequency, showing a 68% drop from 0.01 Hz to the highest frequency of 100 kHz. This suggests a system where none of its components, including the electrolyte and the steel-concrete bar system, presents substantial resistance to the polarization of the electric charges accumulated in the R4 electrodes. Consequently, this affects the protection of the steel reinforcement and allows for increased chloride ion attack on the reinforcement, potentially compromising its structural integrity [22].

The Nyquist plot in Figure 6 represents the RHA concrete sample, which includes rice husk ash addition, maintaining the same water-to-cement ( $w/c$ ) ratio of 0.7.

Analyzing the time evolution of the real component (see Table 12), attributed to the system’s resistance to the corrosive process, and comparing impedances at the low frequency of 10 mHz, we observe an initial decrease from 287 k $\Omega$  to 198 k $\Omega$ . However, from the fourth test onwards, there is an increase from 205 k $\Omega$  to 244 k $\Omega$ , followed by a decrease in the 13th measurement, from 149 k $\Omega$  to 34 k $\Omega$ . This frequency range is associated with resistance (R4), representing the polarization resistance of electrical charges in the region of the armature (electrode)/electrolyte (concrete) interface.

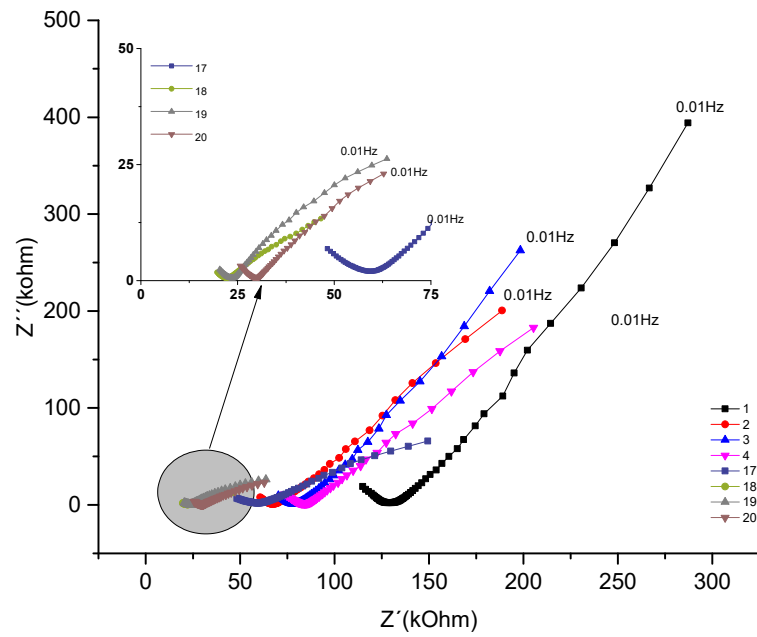


Figure 6. Nyquist plot for the RHA concrete system over a one-year period of NaCl exposure.

Table 12. Real component ( $Z'$ ) for RHA concrete associated with system resistance at three frequencies—100 kHz, 39 Hz, and 0.01 Hz.

Frequency/Hz	CCA-Months/ $Z'$ k $\Omega$																			
	1	2	3	4	5	6	7	8	9	10	11	12	13	14	15	16	17	18	19	20
100 k	114	60	70	73	62	77	81	88	85	74	82	78	84	94	37	48	19	20	25	13
39	131	69	80	85	72	92	97	98	109	106	93	104	100	107	112	47	61	23	24	15
0.01	287	188	198	205	181	212	219	221	244	240	203	222	227	146	118	149	46	63	62	34

At medium frequencies, for example, 39 Hz, the real component initially decreases from 131 k $\Omega$  to 72 k $\Omega$ . Then, from the sixth test, it increases, reaching 112 k $\Omega$  in the 15th measurement. From the 16th measurement, it gradually decreases to 47 k $\Omega$ , eventually reaching 15 k $\Omega$ . This trend is related to the resistance of the bar/concrete system ( $R_2$ ). Compared to the REF material, the addition of pozzolans becomes significant, as discussed in Section 4.1, highlighting their protective effect against chloride attack.

Observing the imaginary component at 10 mHz, an initial decrease in values over time is noted, from 394 k $\Omega$  to 145 k $\Omega$ . From the sixth test onwards, there is an increase from 167 k $\Omega$  to 183 k $\Omega$ , followed by a decrease from the 10th measurement, going from 117 k $\Omega$  down to 10 k $\Omega$ . This component, associated with the system’s reactance, indicates opposition to current flow, as detailed in Table 13.

Table 13. Imaginary component ( $Z''$ ) for RHA concrete associated with system reactance at three frequencies—100 kHz, 39 Hz, and 0.01 Hz.

Frequency/Hz	CCA-Months/ $Z''$ k $\Omega$																			
	1	2	3	4	5	6	7	8	9	10	11	12	13	14	15	16	17	18	19	20
100 k	18	7	9	10	8	12	13	14	16	15	14	17	16	17	15	5	6	1	3	1
39	2	1.74	1.85	1.83	1.57	1.98	2.1	2.13	2.42	2.38	2.3	2.4	2.3	2.49	1.8	1.9	2.4	0.8	0.70	0.74
0.01	394	200	262	182	145	167	183	157	184	183	117	127	121	137	50	66	13	26	23	10

The alterations in the real component, which are associated with the system’s resistance, are visually depicted in Figure 7. This figure illustrates the changes across three selected frequency bands: 0.01 Hz, 39 Hz, and 100 kHz.

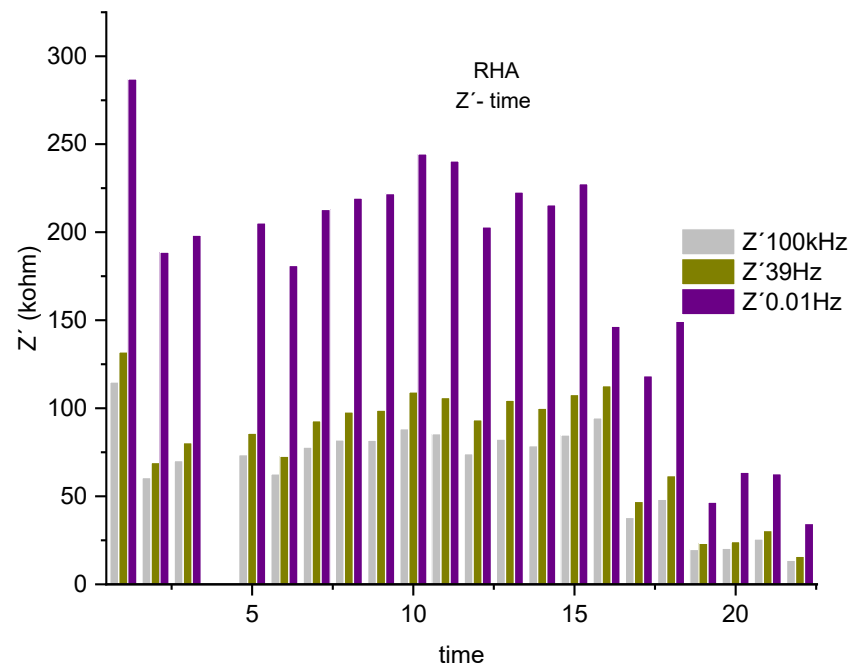


**Figure 7.** Histogram of the real component ( $Z'$ ) for RHA concrete, illustrating system resistance at three frequencies—100 kHz, 39 Hz, and 0.01 Hz.

A noticeable drop in the real component, which is associated with the system's resistance to the corrosive process, is observed at frequencies of 0.01 Hz, 39 Hz, and 100 kHz. Initially, there is a decreasing trend up to the sixth test, followed by an increase as depicted in the impedance spectrum up to the 14th measurement. This phenomenon is consistent across the frequency range from 0.01 Hz to 100 kHz, showing a variation of around 62%. This indicates a system where, at certain times, all its components, such as the electrolyte and the steel-concrete bar system, exhibit an increase in resistance. This effect may be linked to the reduced mobility of chloride ions [8], possibly as a result of the increased matrix density due to the hydration reaction. The hydration is enhanced by the addition of the active mineral, predominantly silicon-based, emphasizing the physical effect.

Following this analysis, the spectra for the MK concrete sample, which contains a 10% metakaolin substitution for cement, are presented through the Nyquist graph.

Observing a Figure 8 the time evolution of the real component, as presented in Table 14, associated with the system's resistance to the corrosive process, especially at low frequencies of 10 mHz, a decreasing trend is evident. Initially, the impedance drops from 337 k $\Omega$  to 170 k $\Omega$  by the sixth measurement. This frequency range is linked to resistance ( $R_4$ ), reflecting the polarization resistance of electrical charges in the area of the bar electrode and electrolyte (concrete). After the seventh measurement, the values show relative stability, fluctuating from 181 k $\Omega$  to 168 k $\Omega$ . Following the 15th measurement, a decrease is noted again, from 168 k $\Omega$  to 92 k $\Omega$  [1].

At medium frequencies, such as 39 Hz, the real component's behavior initially decreases from 147 k $\Omega$  to 107 k $\Omega$  by the fifth measurement. From the sixth test, it stabilizes, remaining around 118 k $\Omega$  to 131 k $\Omega$  until the 15th measurement. After the 16th measurement, a gradual decrease is observed, from 102 k $\Omega$  to 66 k $\Omega$ . This trend may be related to the resistance of the bar/concrete  $R_2$  system. Compared to the REF material, the addition of pozzolans, particularly those based on aluminum-silicon [8], as discussed in Section 4.1, becomes significant, demonstrating a chemico-physical protective effect against chloride attack [14].

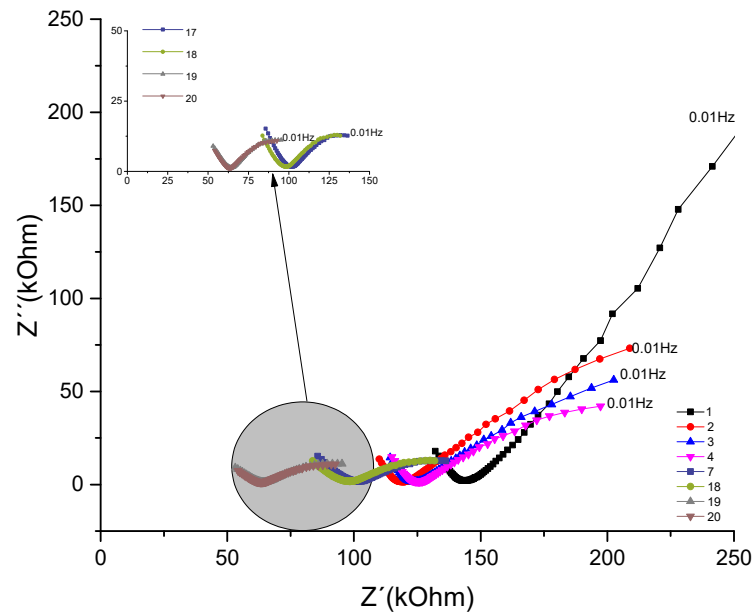


**Figure 8.** Nyquist plot for the MK concrete system over a one-year period with NaCl exposure.

**Table 14.** Real component ( $Z'$ ) for MK concrete associated with system resistance at three frequencies—100 kHz, 39 Hz, and 0.01 Hz.

Frequency/Hz	MK-Months/ $Z'$ k $\Omega$																			
	1	2	3	4	5	6	7	8	9	10	11	12	13	14	15	16	17	18	19	20
100 k	132	109	114	114	97	106	115	119	119	117	112	100	106	100	112	86	83	53	54	55
39	147	121	125	127	107	118	129	133	134	133	129	116	124	119	131	102	99	65	64	66
0.01	337	208	202	197	173	170	181	180	173	171	166	151	161	155	168	136	136	131	95	92

Observing the imaginary component at 10 mHz, an initial decrease is also noted in the values over time, from 337 k $\Omega$  to 170 k $\Omega$ . In the seventh test, there is an increase to 181 k $\Omega$ , followed by a decrease in the eighth measurement, from 180 k $\Omega$  to 92 k $\Omega$ . It is important to note that this component is associated with the system’s reactance, indicating opposition to current flow, which varies with frequency, as detailed in Table 15.

**Table 15.** Imaginary component ( $Z''$ ) for MK concrete associated with system reactance at three frequencies—100 kHz, 39 Hz, and 0.01 Hz.

Frequency/Hz	MK-Months/ $Z''$ k $\Omega$																			
	1	2	3	4	5	6	7	8	9	10	11	12	13	14	15	16	17	18	19	20
100 k	17	13	14	14	11	13	16	16	16	17	18	16	16	17	19	14	12	9	7	8
39	3.1	1.86	1.88	1.84	1.60	1.66	1.75	1.77	1.73	1.81	1.77	1.67	1.81	1.77	1.6	1.8	1.79	1.91	1.71	1.41
0.01	407	73	56	42	39	25	24	22	18	16	16	16	16	15	15	11	12	12	10	10

Figure 9 is presented to visualize the changes previously described in the real component, associated with the system’s resistance in MK concrete. It focuses on three selected frequency bands: 0.01 Hz, 39 Hz, and 100 kHz.

In examining the real component, which is linked to the system’s resistance against the corrosive process, a decreasing trend is observed up to the sixth test, followed by some stability, as delineated in the impedance spectrum up to the 15th measurement. This trend, occurring from the lowest frequency of 0.01 Hz to the highest of 100 kHz, shows a variation of around 39%. This indicates a system where all components, including the electrolyte and the steel-concrete bar system, are active. Notably, the electrolyte resists the passage of chloride ions, which is crucial for maintaining the integrity of the reinforcement.

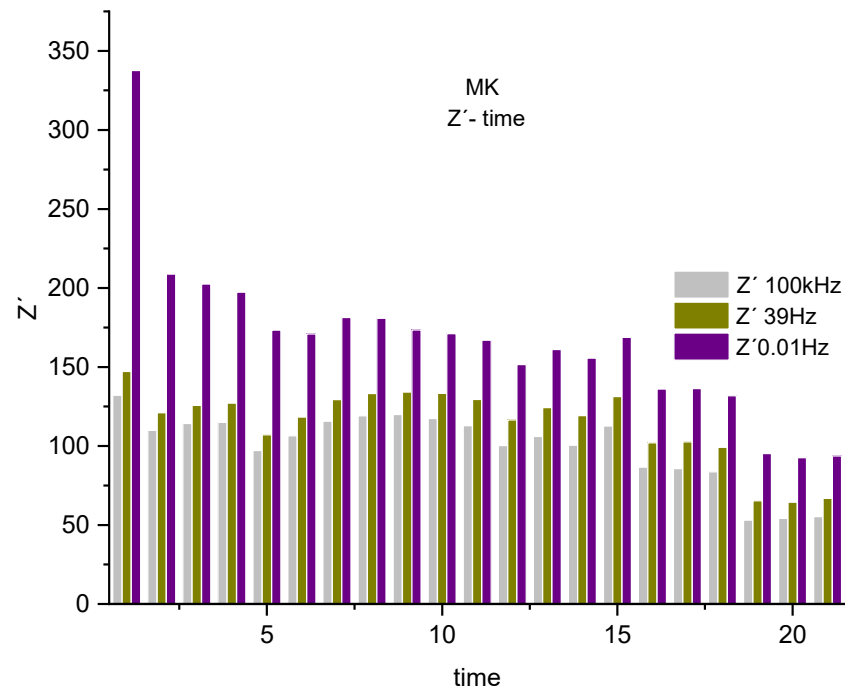


**Figure 9.** Histogram of the real component ( $Z'$ ) associated with the resistance of the MK system at three frequencies—100 kHz, 39 Hz, and 0.01 Hz.

Through the analysis of Nyquist spectra over one year for all three materials (REF, RHA, MK), an equivalent circuit was observed. In principle, this can be represented by a resistance ( $R$ ) in parallel with a pseudo-capacitor ( $Q$ ), with the total circuit comprising four sub-circuits in series. Figure 10 illustrates this representation.

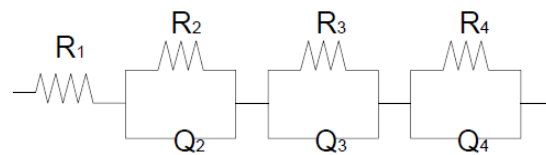


**Figure 10.** Equivalent circuit of the studied system. Source: José Ramón Jurado Egea (JURADO, J. R.), CSIC Madrid.

The equivalent circuit for the studied system can be represented as  $R_1 (R_2Q_2) (R_3Q_3) (R_4Q_4)$ , comprising four sub-circuits. The first sub-circuit corresponds to the electrolyte resistance ( $R_1$ ), while the second represents the semicircle associated with the concrete system plus the steel bar ( $R_2$ ), aligning with the findings in [23]. The third arc is linked to the previous interface plus the diffusion process ( $R_3$ ), and the fourth arc represents the resistance effect of the polarization of electrical charges accumulating at the electrodes ( $R_4$ ). By obtaining the equivalent circuit of the system under study, each parameter obtained in the three materials (REF, RHA, MK) can be evaluated over time (JURADO, J. R.).

Subsequent to obtaining all the impedance spectra, several analyses were conducted. The first involved an analysis of variance (ANOVA) comparison, presented in Table 16, assessing the variance between the groups (REF, RHA, MK) for frequencies 100 kHz, 39 Hz, and 0.01 Hz of the real component over time. This was followed by overlaying them with the previously analyzed frequencies of 100 kHz, 39 Hz, and 0.01 Hz through a histogram for each frequency. The second analysis method was based on calculating the maximum value among the three materials for each chosen frequency. Subsequently, we evaluated the percentage variation of this maximum impedance relative to other lower impedance values [24].

**Table 16.** Analysis of variance of the real component ( $Z'$ ) for REF, RHA, MK associated with system resistance at three frequencies—100 kHz, 39 Hz, and 0.01 Hz.

	Degrees of Freedom	Sum of Squares	Mean Square	F Statistic Value	$p$ -Value
Material	2	294,150.1	147,075.1	64.21	$1.0 \times 10^{-16}$
Frequencies	2	211,040.7	105,520.4	46.07	$1.0 \times 10^{-16}$
Interaction	4	23,182.8	5795.7	2.53	0.04229
Model	8	530,497.1	66,312.1	28.95	$1.0 \times 10^{-16}$
Error	177	405,423.0	2290.5	--	--
Corrected Total	185	935,920.2	--	--	--

The ANOVA shows that at high frequencies of 100 kHz for the three materials (REF, RHA, MK), a significant difference (very small  $p$ -value) is observed when comparing the means. The difference between MK and REF is more pronounced than that between RHA and REF. Additionally, the difference is smaller when comparing RHA to MK.

Moreover, at medium frequencies, a similar pattern is evident among the three materials. The difference in means between MK and REF is again more significant than that between RHA and REF. Furthermore, the difference is less marked when comparing RHA to MK.

In addition, at low frequencies, the differences among the three materials also exhibit a notable pattern. The difference between RHA and REF is greater than that between MK and REF. Notably, there is no significant difference between the RHA and MK groups, suggesting greater similarity in their behavior at these frequencies.

Analysis of the three materials involved in this study, REF, RHA, and MK, is presented in Figures 11–13.

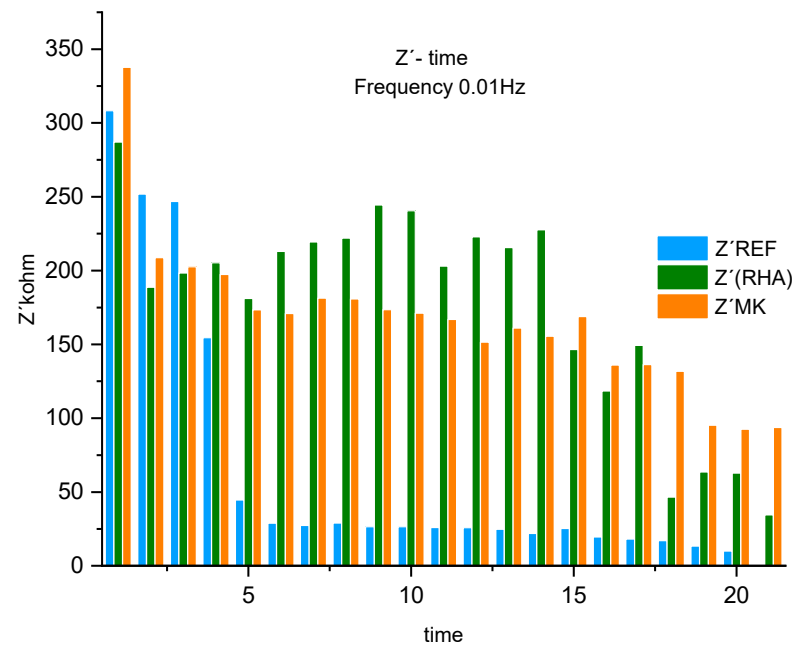


**Figure 11.** Real component of the histogram ( $Z'$ ) associated with system resistance at one frequency, 0.01 Hz, for REF, RHA, and MK.

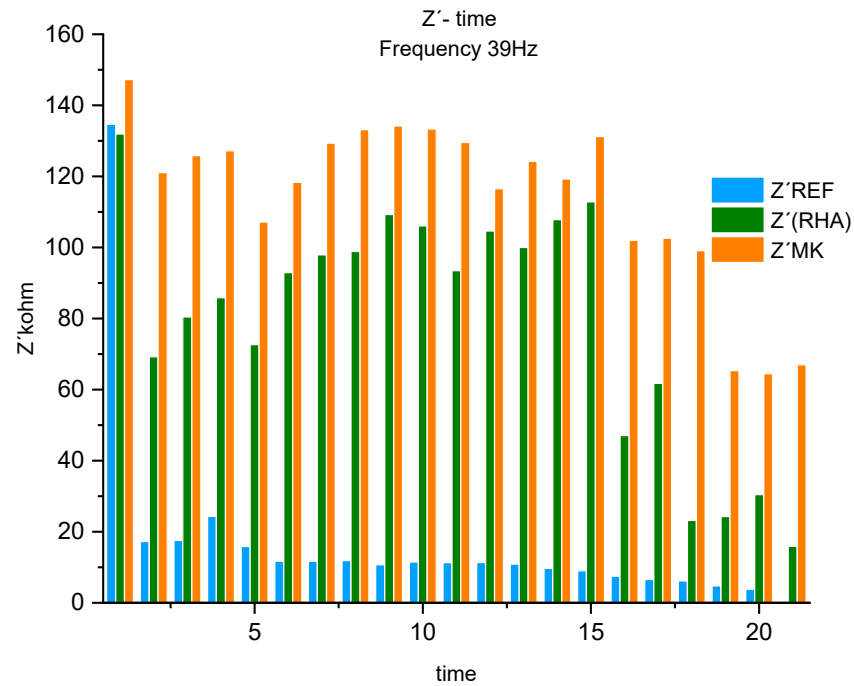


**Figure 12.** Real component of the histogram ( $Z'$ ) associated with system resistance at a single frequency, 39 Hz, for REF, RHA, and MK.

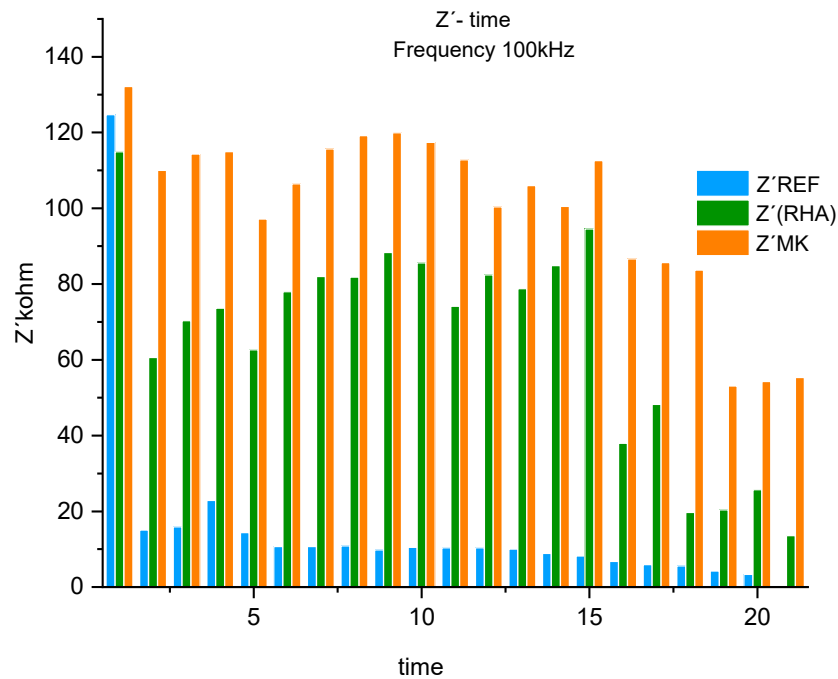


**Figure 13.** Real component of the histogram ( $Z'$ ) associated with system resistance at a single frequency, 100 kHz, for REF, RHA, and MK.

Analyzing the histogram in Figure 11, we can observe the system’s resistance to the polarization of electric charges at low frequencies, specifically in the electrodes (bars/concrete) and charge transfer resistance. Prior to the first measurement, corresponding to the first month of NaCl exposure, MK shows the highest resistance, with a 14% difference compared to RHA and an 8% difference compared to REF. From the second to the third measurement, REF exhibits the highest resistance, differing by 22% from RHA and 17% from MK. This may be attributed to the delay in the hydration process of cement grains caused by active additions in concretes with pozzolanic material compared to standard concrete [10].

These initial measurements suggest a variation in the cement hydration process across the materials [22].

From the fourth to the thirteenth measurement, RHA shows the maximum resistance, with a difference from REF of 24% in the fourth measurement and varying up to 86% by the thirteenth. The difference between RHA and MK was 4% in the fourth and fifth measurements and increased to 27% by the thirteenth. This indicates an increase in resistance for MK and RHA compared to REF, potentially reflecting the efficiency of pozzolanic additions in resisting chloride ion penetration, possibly favoring physical over chemical processes [21,25,26].

From the fourteenth to the twentieth measurement, MK exhibits the highest resistance compared to the other materials. The difference between MK and REF is 88%, remaining consistent until the last measurement. When MK is compared with RHA, the difference varies, starting at 5% and reaching 63% in subsequent measurements. This suggests that a chemical phenomenon may be dominating the system's resistance rather than physical factors, as indicated in the tomography title. Although RHA material has lower porosity than MK, which would be significant if the dominant process were physical over chemical, the results from the chloride diffusion test and EIS indicate that chemical processes are predominantly resisting chloride ion penetration [14,26].

Analyzing the histogram in Figure 12 for the three materials (REF, RHA, MK) at a frequency of 39 Hz, which falls within the medium frequency range and relates to the concrete bar system (bars/concrete), we observe specific trends. The maximum value in the first measurement, corresponding to the first month of NaCl exposure, through to the 20th measurement, consistently belongs to the MK concrete system. Comparing MK with REF, there is an 8% difference in the first measurement, which then stabilizes to an average difference of around 90%, fluctuating from 85% and gradually increasing to 94%. This indicates that the REF concrete system offers minimal protection (resistance) against the passage of chloride ions.

When comparing MK with RHA concrete, the first measurement shows a 10% difference between their resistances. From the second measurement onwards, this difference begins to oscillate, showing an average difference of 42% between the second and fifth measurements, which then decreases to 21% from the sixth to the eleventh measurements. The difference further drops to 10% from the twelfth to the fifteenth measurements. From the sixteenth and seventeenth measurements, there is an increase to 53%, and finally, from the eighteenth to the twentieth measurement, it rises again to 76%. This pattern suggests a decrease in RHA material's resistance to the aggressive agent, implying that the behavior may be related to a dominant chemico-physical domain at the steel/concrete interface, becoming more pronounced after the fifteenth measurement, around the eighth month of exposure [8].

In the final analysis, examining the histogram for the three materials (REF, RHA, MK) in Figure 13 at a frequency of 100 kHz, which falls within the high frequency range and relates to the electrolyte resistance (concrete + water + NaCl), we observe consistent trends. From the first measurement, corresponding to the first month of NaCl exposure, to the 20th measurement, the maximum resistance is consistently observed in the MK concrete. This shows a 6% difference in resistance compared to REF in the first measurement, and from the second measurement onwards, a steady difference of about 90% on average is maintained, fluctuating from 86% and increasing up to 94%. This suggests that REF material offers minimal protection (resistance) against the passage of chloride ions.

When comparing MK concrete to RHA concrete, the first measurement shows a 13% difference between their resistances. From the second measurement, this difference begins to fluctuate, displaying an average difference of 38% from the second to fifth measurements, then decreasing to 27% from the sixth to the thirteenth measurement, and further decreasing to 6% from the fourteenth measurement. From the fifteenth to the sixteenth measurements, the difference increases to 44%, and finally, from the seventeenth to the twentieth measurement, it rises again to 67%. This pattern quantitatively justifies

a resistance system related to a predominantly chemico-physical process, which intensified from the fifteenth measurement onwards.

#### 4.4. Summary of Key Findings

##### Accelerated Chloride Diffusion Tests (ASTM 1556):

The diffusion tests align with previous studies, indicating that pozzolanic additions, particularly those based on aluminum and aluminum-silicon, effectively reduce chloride attacks on steel reinforcement. This effect is less pronounced with silicon-based pozzolans. The results highlight the benefits of active mineral additions, especially aluminum-based ones, in environments exposed to chlorides, such as marine areas.

##### Tomography Analysis:

The reduction in porosity of concrete with pozzolanic additions compared to standard concrete is attributed to specific physicochemical reactions among the mixture's components. These reactions affect the content and nature of the concrete's fractions, influencing their siliceous or calcareous properties, and acidic or basic chemical characteristics. Concrete with mineral additions, such as RHA and MK, forms a denser matrix than conventional Portland cement concrete (REF), enhancing the physical protection against chloride ion ingress. Specifically, RHA concrete, with silicon-based additions, is observed to be less porous compared to MK concrete, which is based on aluminum-silicate.

##### Electrochemical Impedance Spectroscopy (EIS) Analysis:

In the REF concrete system, a notable decrease in the real impedance component over one year of NaCl exposure was observed, indicating reduced system resistance to corrosion. This trend was evident at low and medium frequencies, with an overall 68% drop in resistance, suggesting reduced protection of the steel reinforcement and increased vulnerability to chloride attack.

For RHA concrete, varying trends in the real impedance component over time reflected changes in the system's resistance to corrosion. Initial resistance decrease, followed by an increase and subsequent decrease, was associated with the R4 resistance at the electrode/electrolyte interface. The silicon-based RHA concrete demonstrated protective effects against chloride attack, indicated by the resistance increase over time.

The MK concrete system showed a decreasing trend in system resistance, especially at low frequencies. This decrease in impedance suggested reduced resistance to corrosion induced by NaCl. The aluminum-silicate-based MK concrete exhibited significant protective effects against chloride attack, as evidenced by the consistent decrease in system resistance over time.

## 5. Conclusions

- In utilizing tomography, this study found varying porosity levels across different concrete types. REF concrete exhibited the highest total porosity at 2.48%, MK concrete showed a slightly lower porosity at 2.43%, and RHA concrete had the lowest porosity at 1.06%. These findings are crucial in understanding the microstructural differences among the concretes and their potential impact on durability.
- The chloride diffusion coefficients, determined according to ASTM 1556, varied significantly among the concrete types. REF concrete had the highest diffusion rate ( $D_a = 8.45 \times 10^{-11} \text{ m}^2/\text{s}$ ), indicating a greater vulnerability to chloride penetration, whereas RHA ( $D_a = 1.63 \times 10^{-11} \text{ m}^2/\text{s}$ ) and MK concrete ( $D_a = 9.29 \times 10^{-12} \text{ m}^2/\text{s}$ ) demonstrated considerably lower diffusion rates, suggesting enhanced resistance to chloride ion ingress.
- Electrochemical Impedance Spectroscopy (EIS) effectively characterized and quantified the differences in system resistance among the concrete types. These differences highlight the distinct electrochemical behaviors of the concretes and their responses to corrosive environments.

- At low frequencies (around 0.01 Hz), associated with the resistance in the electrode bars/concrete system, the study identified a blend of physical and chemical resistance, with a slightly greater emphasis on physical mechanisms.
- Medium frequencies (around 39 Hz) were linked to the resistance of the concrete/bar system, revealing a balance of chemical and physical resistance, but with chemical processes playing a more dominant role.
- At high frequencies (around 100 kHz), corresponding to the electrolyte resistance in the system (concrete + water + NaCl), the findings suggest a nuanced balance of physical and chemical protective mechanisms, with a slight lean towards physical protection.
- The addition of active mineral additives, particularly those with an alumino-silicic composition, significantly enhances the concrete's defense against chloride ion attacks. This study illustrates the effectiveness of these additives in providing a predominantly physico-chemical protective effect.

**Author Contributions:** Conceptualization, A.O.D., R.D.T.F. and J.A.d.C.P.G.; Methodology, A.O.D., R.D.T.F. and J.A.d.C.P.G.; Investigation, A.O.D., E.A.d.S. and A.B.d.S.; Software and Validation, A.O.D. and R.d.S.S.; Writing, Review and Editing, A.O.D. and A.B.d.S. Supervision, R.D.T.F. and J.A.d.C.P.G. All authors have read and agreed to the published version of the manuscript.

**Funding:** This research received no external funding.

**Data Availability Statement:** The raw data supporting the conclusions of this article will be made available by the authors on request.

**Conflicts of Interest:** The authors declare no conflict of interest.

## References

1. Ribeiro, D.V. Use of Electrochemical Impedance Spectroscopy (EIS) to monitoring the corrosion of reinforced concrete para monitoramento da corrosão em concreto armado. *Rev. IBRACON De Estrut. E Mater.* **2015**, *8*, 529–537. [[CrossRef](#)]
2. Zhou, Y.; Gencturk, B.; Willam, K.; Attar, A. Carbonation-Induced and Chloride-Induced Corrosion in Reinforced Concrete Structures. *J. Mater. Civ. Eng.* **2015**, *27*, 04014245. [[CrossRef](#)]
3. Figueira, R.B. Electrochemical Sensors for Monitoring the Corrosion Conditions of Reinforced Concrete Structures: A Review. *Appl. Sci.* **2017**, *7*, 1157. [[CrossRef](#)]
4. Ismail, M.; Ohtsu, M. Corrosion rate of ordinary and high-performance concrete subjected to chloride attack by AC impedance spectroscopy. *Constr. Build. Mater.* **2006**, *20*, 458–469. [[CrossRef](#)]
5. Tutti, K. *Corrosion of Steel in Concrete*; Swedish Cement and Concrete Research Institute: Stockholm, Sweden, 1982; pp. 17–21.
6. Chi, Z.; Wang, L.; Lu, S.; Zhao, D.; Yao, Y. Development of mathematical models for predicting the compressive strength and hydration process using the EIS impedance of cementitious materials. *Constr. Build. Mater.* **2019**, *208*, 659–668. [[CrossRef](#)]
7. Helene, P.; Terzian, P. *Manual de Dosagem e Controle do Concreto*; PINI/SENAI: São Paulo, Brasil, 1993; p. 349.
8. Talero, R.; Pedrajas, C.; Delgado, A.; Rahhal, V. Re-use of incinerated agro-industrial waste as pozzolanic addition. *Comp. Span. Silica Fume. Mater. De Construcción* **2009**, *59*, 53–89. [[CrossRef](#)]
9. ASTM C 1559; Standard test method for determining the apparent chloride diffusion coefficient of cementitious mixture by bulk diffusion. ASTM International: West Conshohocken, PA, USA, 2022.
10. Banthia, N.; Zanotti, C.; Sappakittipakorn, M. Sustainable fiber reinforced concrete for repair applications. *Constr. Build. Mater.* **2014**, *67*, 405–412. [[CrossRef](#)]
11. 83992-1:2012 EX; UNE, Durabilidad Del Hormigón. Métodos de Ensayo. Ensayos de Penetración de Cloruros En El Hormigón. Parte 1: Método Natural Para La Determinación Del Tiempo Hasta Corrosión, AENOR. The Spanish Association for Standardization and Certification: Madrid, Spain, 2012.
12. Mark, E. Orazem Bernard Tribollet. In *Electrochemical Impedance Spectroscopy*; John Wiley & Sons, Inc.: Hoboken, NJ, USA, 2008.
13. Rentería, R.M. Contribución al estudio analítico y físico-químico del sistema cementos portland -puzolanas y escoria siderúrgica-cloruros y agua. *Inf. De La Construcción* **1997**, *49*, 73.
14. Talero, R.; Trusilewicz, L.; Delgado, A.; Pedrajas, C.; Lannegrand, R.; Rahhal, V.; Mejía, R.; Delvasto, S.; Ramírez, F.A. Comparative and semi-quantitative XRD analysis of Friedel's salt originating from pozzolan and Portland cement. *Constr. Build. Mater.* **2011**, *25*, 2370–2380. [[CrossRef](#)]
15. Chung, S.Y.; Kim, J.S.; Stephan, D.; Han, T.S. Overview of the use of micro-computed tomography (micro-CT) to investigate the relation between the material characteristics and properties of cement-based materials. *Constr. Build. Mater.* **2019**, *229*, 116843. [[CrossRef](#)]
16. Diamond, S.; Wild, S. A discussion of the paper Mercury porosimetry—An inappropriate method for the measurement of pore size distributions in cement-based. *Cem. Concr. Res.* **2001**, *31*, 1657–1658.

17. Khatib, J.M.; Wild, S. Pore size distribution of metakaolin paste. *Cem. Concr. Res.* **1996**, *26*, 1545–1553. [[CrossRef](#)]
18. du Plessis, A.; Olawuyi, B.J.; Boshoff, W.P.; le Roux, S.G. Simple and fast porosity analysis of concrete using X-ray computed tomography. *Mater. Struct./Mater. Et Constr.* **2016**, *49*, 553–562. [[CrossRef](#)]
19. Park, K.B.; Kwon, S.J.; Wang, X.Y. Analysis of the effects of rice husk ash on the hydration of cementitious materials. *Constr. Build. Mater.* **2016**, *105*, 196–205. [[CrossRef](#)]
20. Zain, M.F.M.; Islam, M.N.; Mahmud, F.; Jamil, M. Production of rice husk ash for use in concrete as a supplementary cementitious material. *Constr. Build. Mater.* **2011**, *25*, 798–805. [[CrossRef](#)]
21. Mobasher, B.; Shekarchi, M.; Bonakdar, A.; Bakhshi, M.; Mirdamadi, A. Transport properties in metakaolin blended concrete. *Constr. Build. Mater.* **2010**, *24*, 2217–2223. [[CrossRef](#)]
22. Figueiredo, C.P.; Santos, F.B.; Cascudo, O.; Carasek, H.; Cachim, P.; Velosa, A. The role of metakaolin in the protection of concrete against the deleterious action of chlorides O papel do metacaulim na proteção dos concretos contra a ação deletéria de cloretos. *Rev. IBRACON De Estrut. E Mater.* **2014**, *7*, 685–708. [[CrossRef](#)]
23. Sousa, M.A.M. Modelos de Circuitos Equivalentes Para Explicar Espectros de Impedância de Dispositivos de Efeito de Campo. Master's Thesis, Instituto de Física de São Carlos, Basel, Spain, June 2013.
24. Poon, C.S.; Kou, S.C.; Lam, L. Compressive strength, chloride diffusivity and pore structure of high performance metakaolin and silica fume concrete. *Constr. Build. Mater.* **2006**, *20*, 858–865. [[CrossRef](#)]
25. Sakai, Y. Relationship between pore structure and chloride diffusion in cementitious materials. *Constr. Build. Mater.* **2019**, *229*, 116868. [[CrossRef](#)]
26. Saraswathy, V.; Song, H.W. Corrosion performance of rice husk ash blended concrete. *Constr. Build. Mater.* **2007**, *21*, 1779–1784. [[CrossRef](#)]

**Disclaimer/Publisher's Note:** The statements, opinions and data contained in all publications are solely those of the individual author(s) and contributor(s) and not of MDPI and/or the editor(s). MDPI and/or the editor(s) disclaim responsibility for any injury to people or property resulting from any ideas, methods, instructions or products referred to in the content.